Optik - International Journal for Light and Electron Optics 185 (2019) 930–935

Contents lists available at ScienceDirect

Optik

journal homepage: www.elsevier.com/locate/ijleo

Original research article

Transmittance spectrum in a 1D photonic crystal composed fused silica and sea water

Francis Segovia-Chaves[a,b,*], Herbert Vinck-Posada[a], Vigneswaran Dhasarathan[c], M.S. Mani Rajan[d]

[a] Grupo de Óptica e Información Cuántica, Departamento de Física, Universidad Nacional de Colombia, AA 055051 Bogotá, Colombia
[b] Grupo de Física Teórica, Programa de Física, Universidad Surcolombiana, AA 385 Neiva, Colombia
[c] Department of Electronics and Communication Engineering, Sri Krishna College of Technology, Coimbatore, Tamil Nadu 641042, India
[d] Department of Physics, Anna University, Ramanathapuram, India

ARTICLE INFO

Keywords:
Photonic crystal
Temperature
Salinity
Defect mode

ABSTRACT

In this work, the simultaneous sensing process to detect the salinity and temperature for the given water samples using 1D photonic crystal (PC) periodic structure is numerically investigated. The sensing analytes is considered as defect mode and the whole structure is then tuned to observe the transmittance spectrum over the visible region for the different concentration and temperature of water samples. The observation point is noted as peak wavelength spectral shift over the visible region of band gap spectrum. As a simultaneous sensing process, the salinity concentration is detected for the constant temperature of water samples and salt content of samples kept as constant for detecting the temperature point.

1. Introduction

There has been some specific point to develop the fabrication process of photonic band gap (PBG) materials at the optical frequencies. The propagation does not take place in that periodic structured materials. The reason for cutoff propagation in that region has given the attention to evolve the photonic bandgap materials in various applications [1,2]. In 1950, the optical pulse propagation through those periodic materials was deeply analyzed by transfer matrix method (TMM) [3–5]. With the help of TMM, transmittance or reflection spectrum over the given periodic band gap region were analyzed and this studies is extended to the different periodic multi layered structure by means of stacked pattern is so called as photonic crystals (PC's) [6–8] in which the existence of PBG could be found. Though the 2D or 3 PC has been involved for various applications, the fabrication of feasibility like high index contrast and testing precision particularly in the visible region is quite complex. Hence, the overall attention was turned to the 1D PC structure with the simple fabrication process and it was inferred that does not support of omnidirectional while following the Brewster effect. Causing the unique property, many 1D Devices was explored such as reflector [9], filter [10,11], multiplexer [12], switches [13], resonator [14], refractometric [15], polarization controller [16], etc. As the fabrication of 1D PC for both visible and IR region has been considered as much compatible with its scaling factor from micro scale to nano scale [17], the PC based optical sensor has attracted from the many researchers in the photonic society. With that aids, defective or cavity based PC [18–26] has been explored such as optical transducer for biosensor [27], terahertz gas sensing [28], chemical sensing [29], temperature [30], and hydrostatic pressure [31]. In continuation, refractive index based sensors [32] using 1D are proposed and its sensitivity is

* Corresponding author at: Grupo de Física Teórica, Universidad Surcolombiana-Neiva (Huila), Colombia.
E-mail address: francis.segoviac@gmail.com (F. Segovia-Chaves).

https://doi.org/10.1016/j.ijleo.2019.03.110
Received 1 February 2019; Accepted 19 March 2019

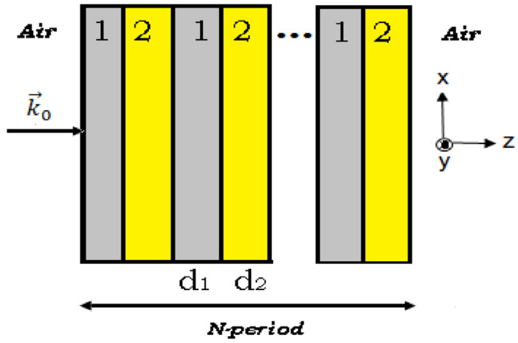

Fig. 1. Structure of the regular 1D PC (without defects).

calculated by peak wavelength shift happening in the output transmission spectrum for its variation of different concentration of samples or the refractive indices of given samples. Recently, few researchers have proposed the refractive index sensor for temperature [33], plasmon-polariton [34], diffraction grating plasmonic sensor [35], single frequency sensor [36] and grating sensor [37]. In 2018 [38], Ramanujam, et al. has proposed the refractive index sensor for cancer cell by introducing defect layer with exertion of mode function in the band gap region and reported its sensitivity as 43 nm/RIU. But there were no literature to propose the dual refractive index sensor using 1D photonic crystal defective structures. In this article, the proposed multilayers periodic 1D PC correlates the numerical procedure of simultaneous detection for the salt concentration and temperature of given water samples. They sensing principle and the detection process is successfully accomplished by the TMM.

2. Theoretical model

Fig. 1 displays the diagram of the one-dimensional photonic crystal (1D-PC) embedded in air with N-periodicity on axis z, which comprises fused silica (layer 1) and sea water (layer 2). The refractive indexes of the media are n_1 and n_2, respectively. Layer thicknesses are represented by d_1 and d_2. Herein, we denote incidence of light with wave vector $\vec{k}_0$. The number of bilayer periods is represented by N.

The refractive index for fused silica is a function of wavelength (λ) and temperature (T) [39], and it is given by

$$n_1^2(\lambda, T) = (1.31552 + 6.90754 \times 10^{-6}T) + \frac{(0.788404 + 23.5835 \times 10^{-6}T)\lambda^2}{\lambda^2 - (0.0110199 + 0.584758 \times 10^{-6}T)} + \frac{(0.91316 + 0.548368 \times 10^{-6}T)\lambda^2}{\lambda^2 - 100} \tag{1}$$

The refractive index for sea water is a function of salinity (s), as per the following formula [40],

$$n_2(s, \lambda, T) = 1.3140 + (1.779 \times 10^{-4} - 1.05 \times 10^{-6}T + 1.6 \times 10^{-8}T^2)s - 2.025835 \times 10^{-6}T^2 + \frac{15.868 + 0.01155s - 0.00423T}{\lambda} - \frac{4382}{\lambda^2} + \frac{1.1455 \times 10^{-6}}{\lambda^3} \tag{2}$$

In this work, the transfer-matrix method (TMM) will be used to calculate the transmittance spectrum of 1D-PC [41,42]. In the TMM, the total matrix of the structure represented in Fig. 1 is provided by,

$$\mathbf{M} = \begin{pmatrix} m_{11} & m_{12} \\ m_{21} & m_{22} \end{pmatrix} = \mathfrak{D}_a^{-1}[\mathfrak{D}_1\mathfrak{P}_1\mathfrak{D}_1^{-1}\mathfrak{D}_2\mathfrak{P}_2\mathfrak{D}_2^{-1}]^N\mathfrak{D}_a \tag{3}$$

where $\mathfrak{D}_j$ is the dynamic matrix for the j-th layer (with $j = 1, 2$) with a thickness of d_j, and it is represented by

$$\mathfrak{D}_j = \begin{pmatrix} 1 & 1 \\ n_j & -n_j \end{pmatrix} \tag{4}$$

where n_j is the refractive index of the j-th layer. The dynamic air matrix is $\mathfrak{D}_a$ ($n_a = 1.0$), and the propagation matrix is

$$\mathfrak{P}_j = \begin{pmatrix} e^{i\varphi_j} & 0 \\ 0 & e^{-i\varphi_j} \end{pmatrix} \tag{5}$$

where the phase is $\varphi_j = \frac{2\pi d_j}{\lambda}n_j$. The Γ transmittance may be calculated with the m_{11} matrix elements from Eq. (1),

$$\Gamma = \left|\frac{1}{m_{11}}\right|^2 \tag{6}$$

When a defect D is introduced into the structure, the translation symmetry of the 1D-PC is broken. Fig. 2 displays the defective 1D-PC with the defect D of d_D thickness.

In this case, the total matrix of the defective structure is given by

$$\mathbf{M} = \mathfrak{D}_a^{-1}[\mathfrak{D}_1\mathfrak{P}_1\mathfrak{D}_1^{-1}\mathfrak{D}_2\mathfrak{P}_2\mathfrak{D}_2^{-1}]^N\mathfrak{D}_D\mathfrak{P}_D\mathfrak{D}_D^{-1}[\mathfrak{D}_1\mathfrak{P}_1\mathfrak{D}_1^{-1}\mathfrak{D}_2\mathfrak{P}_2\mathfrak{D}_2^{-1}]^N\mathfrak{D}_a \tag{7}$$

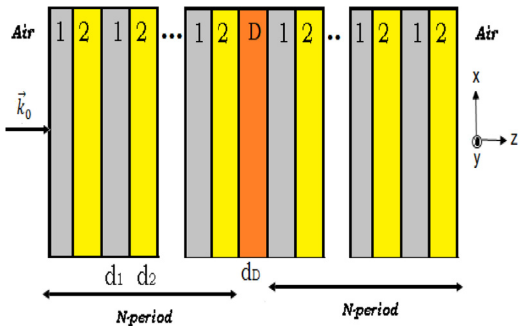

Fig. 2. Structure of the defective 1D-PC, where D is the defect with d_D thickness.

The Γ transmittance is calculated using Eq. (6) and accounting for the matrix elements from Eq. (7).

3. Numerical results and discussion

Fig. 3 displays the effect of temperature on the transmittance spectrum of the regular 1D-PC (without defects). The values used for the simulations are as follows: the number of bilayers $N = 15$, salinity $s = 0.0$, and layer thicknesses $d_1 = 1000$ nm and $d_2 = 500$ nm. Fig. 3(a) shows the transmittance spectrum when increasing temperature from 20 °C to 100 °C. The spectrum has a very small shift towards regions of shorter wavelengths, as shown in Fig. 3(b).

At $T = 25$ °C, the two transmittance gaps are located in the wavelength ranges 790.39–808.17 nm and 946.98–975.46 nm. At $T = 55$ °C, the gaps shift to shorter wavelengths; the first gap is located between 789.41 nm and 807.67 nm and the second gap is located between 945.9 nm and 974.36 nm.

A transmittance spectrum shift towards regions of longer wavelengths when we increase salinity and maintain constant temperature at 25 °C is noteworthy, as shown in Fig. 4(a). When increasing salinity by 0.5, the two transmittance gaps are located in the regions from 799.6 nm to 815.17 nm and from 956.25 nm to 984.88 nm, as shown in Fig. 4(b).

Fig. 5 displays, in two panels, the effects on the transmittance spectrum when increasing the thicknesses of the materials at constant temperature (25 °C) and salinity (0.5) values.

Fig. 5(a) shows the transmittance spectrum when maintaining $d_2 = 500$ nm constant and increasing d_1 from 500 to 1000 nm. Fig. 5(b) presents the spectrum for a fixed $d_1 = 500$ nm value and increasing d_2 from 100 to 600 nm. In both cases, the gaps shift to regions of longer wavelengths when the layer thicknesses increase for the material.

When breaking the periodicity of the 1D-PC by inserting a defective sea water layer of d_D thickness, a resonance peak, known as defect mode, is created within the gap. Fig. 6 (a) displays the transmittance spectrum for the defective crystal when temperature increases from 20 °C to 100 °C at a constant salinity of 0.5 and constant layer thicknesses of $d_1 = d_2 = 500$ nm and $d_D = 200$ nm. We observe that at $T = 20$ °C, the height of the defective mode is 0.93 and it is located at 1037.59 nm. As temperature increases, the defective mode shifts to regions of shorter wavelengths. In Fig. 6(b), at $T = 50$ °C, the defective mode is located at 1036.46 nm.

In the following calculations, temperature ($T = 20$ °C) and thicknesses ($d_D = 200$ nm and $d_1 = d_2 = 500$ nm) remain constant, while salinity increases from 0.0 to 1.0. In Fig. 7(a), the defective mode presents a shift towards regions of longer wavelengths as

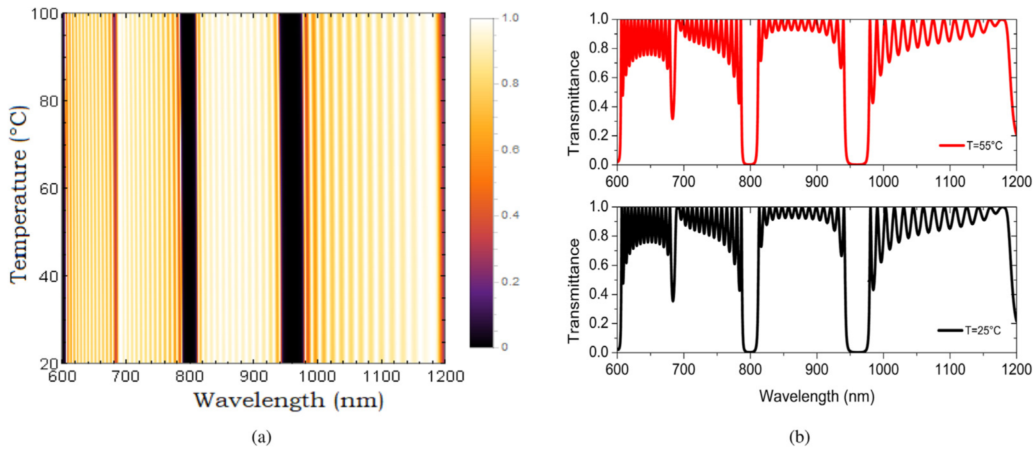

Fig. 3. (a) Transmittance spectrum for the temperature increment from 20 °C to 100 °C. (b) Transmittance spectrum between temperatures of 25 °C (black line) and 55 °C (red line). The values used in the simulations are $s = 0.0$, $N = 15$, $d_1 = 1000$ nm and $d_2 = 500$ nm. (For interpretation of the references to color in this figure legend, the reader is referred to the web version of this article.)

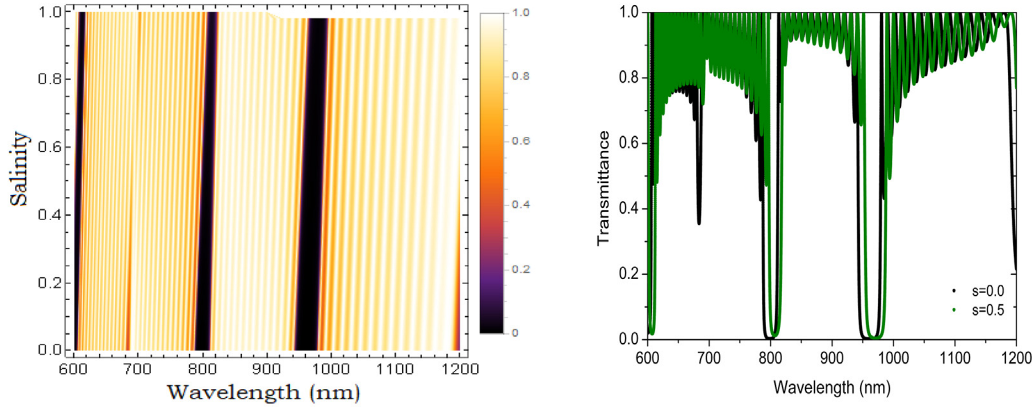

(a) (b)

Fig. 4. (a) Effect of salinity increment from 0 to 1.0 on the transmittance spectrum. (b) Transmittance spectrum for salinity of 0.0 (black line) and 0.5 (green line). The values used in the simulations are $T = 25\,^{\circ}\mathrm{C}$, $N = 15$, $d_1 = 1000$ nm and $d_2 = 500$ nm. (For interpretation of the references to color in this figure legend, the reader is referred to the web version of this article.)

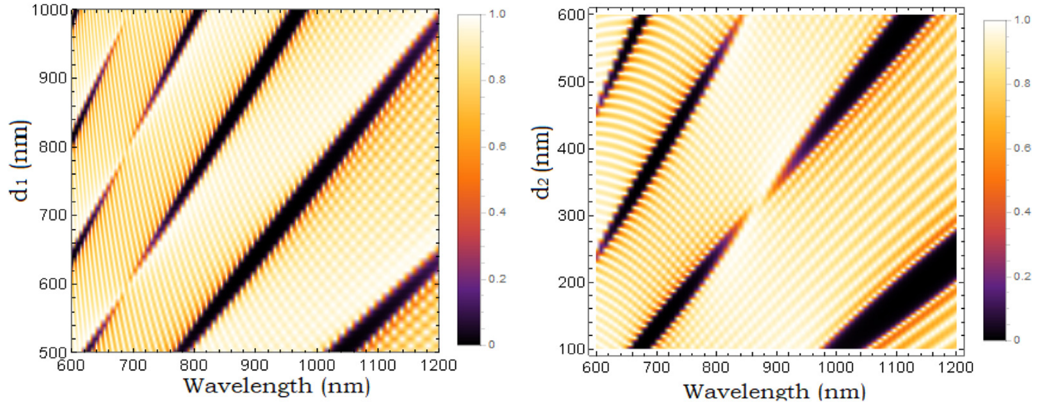

(a) (b)

Fig. 5. Effect on the transmittance spectrum due to increasing layer thicknesses at $T = 25\,^{\circ}\mathrm{C}$, $N = 15$ and $s = 0.5$. (a) Transmittance spectrum as a function of d_1 increase, with $d_2 = 500$ nm. (b) Transmittance spectrum as a function of d_2 increase, with $d_1 = 500$ nm.

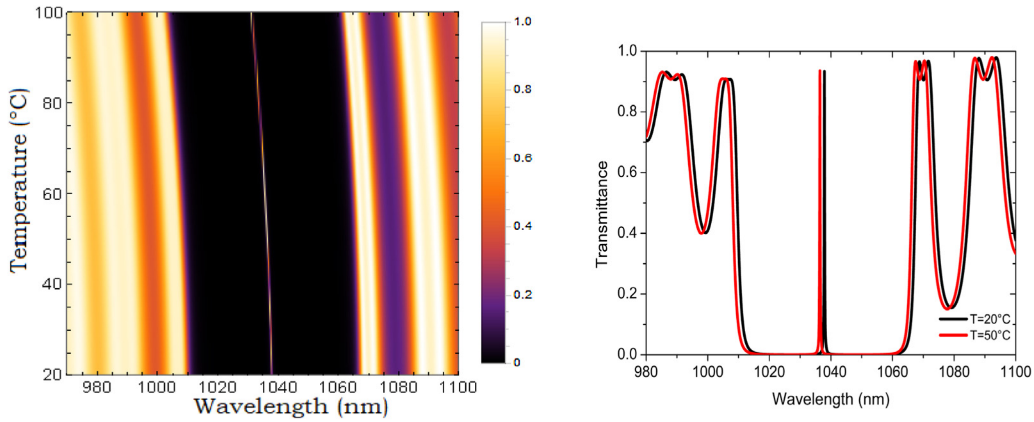

(a) (b)

Fig. 6. (a) Transmittance spectrum of the defective 1D-PC when temperature was increased from 20 °C to 100 °C. (b) Transmittance spectrum of the defective 1D-PC at temperatures of 20 °C (black line) and 50 °C (red line). The values used in the simulations are $s = 0.5$, $N = 15$, $d_D = 200$ nm and $d_1 = d_2 = 500$ nm. (For interpretation of the references to color in this figure legend, the reader is referred to the web version of this article.)

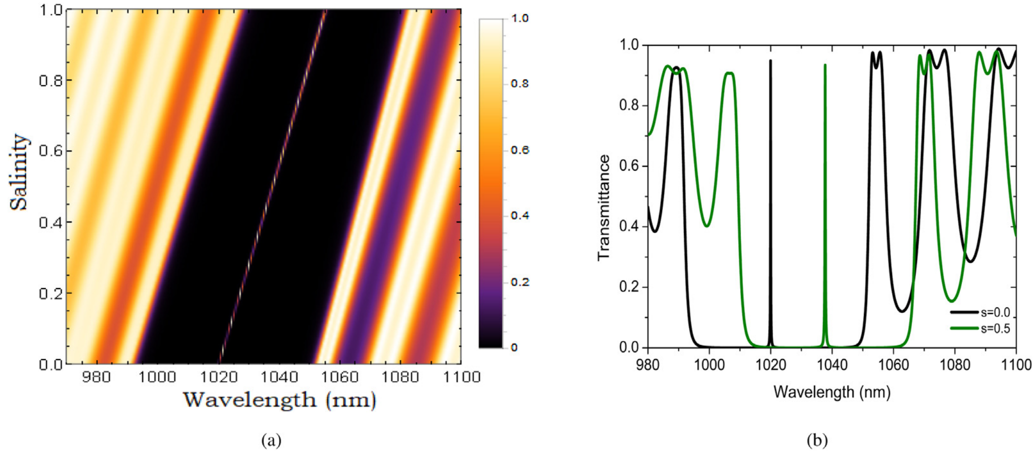

Fig. 7. (a) Transmittance spectrum of the defective 1D-PC when salinity was increased from 0 to 1.0. (b) Transmittance spectrum of the defective 1D-PC at $s = 0.0$ (black line) and $s = 0.5$ (green line). The values used in the simulations are $T = 20\,^{\circ}\mathrm{C}$, $N = 15$, $d_D = 200$ nm and $d_1 = d_2 = 500$ nm. (For interpretation of the references to color in this figure legend, the reader is referred to the web version of this article.)

salinity increases. For $s = 0.0$, the defective mode is located at 1019.2 nm, which shifts to a wavelength of 1037.59 nm when increasing s to 0.5, as shown in Fig. 7(b).

Finally, we address the influence from the defective layer thickness on the transmittance spectrum at values of $T = 25\,^{\circ}\mathrm{C}$, $s = 0.5$, and thicknesses of $d_1 = d_2 = 500$ nm. A shift towards regions of longer wavelengths is reported when increasing d_D from 100 to 300 nm, as shown in Fig. 8(a). For $d_D = 100$ nm, the defective mode is located at 1021.67 nm. However, for $d_D = 300$ nm, the defective mode is located at 1054.07 nm, as shown in Fig. 8(b).

4. Conclusions

The proposed design for the simultaneous sensing of salinity and temperature using 1D photonic crystal (PC) periodic were numerically investigated using transfer matrix method (TMM). The detection process was achieved by calculating the peak wavelength in the resulted transmission spectrum while varying the samples of sea water. During the detection process of salinity concentration, the temperature of the samples was kept as constant and viceversa.

Acknowledgements

F.S.-Ch. and H.V.-P gratefully acknowledge funding by COLCIENCIAS projects: “Emisión en sistemas de Qubits Superconductores acoplados a la radiación. Código 110171249692, CT 293-2016, HERMES 31361” and “Control dinámico de la emisión en sistemas de Qubits acoplados con cavidades no-estacionarias, HERMES 41611”. F.S.-Ch. also acknowledges to Vicerrectoría de Investigación,

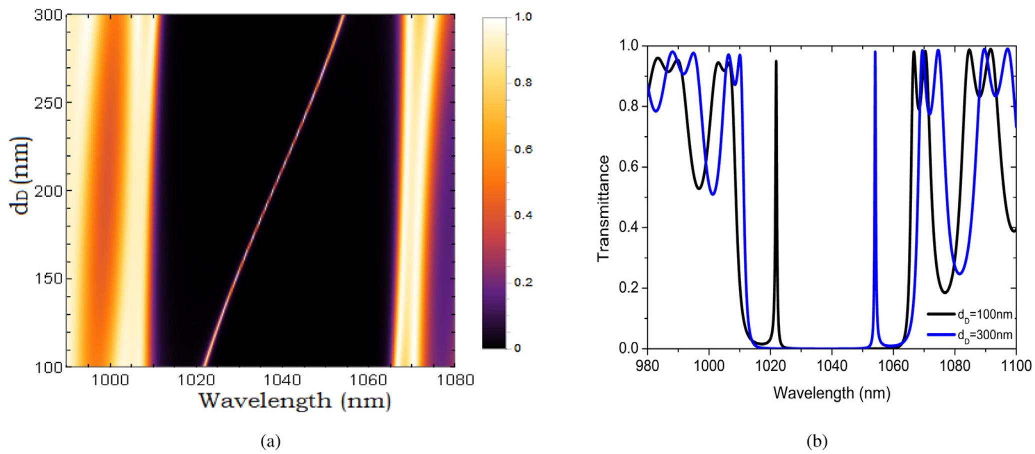

Fig. 8. (a) Transmittance spectrum of the defective 1D-PC when d_D thickness increases from 100 to 300 nm. (b) Transmittance spectrum of the defective 1D-PC for $d_D = 100$ nm (black line) and $d_D = 300$ nm (blue line). The values used in the simulations are $T = 25\,^{\circ}\mathrm{C}$, $N = 15$, $s = 0.5$ and $d_1 = d_2 = 500$ nm. (For interpretation of the references to color in this figure legend, the reader is referred to the web version of this article.)

Universidad Surcolombiana Neiva-Huila.

References

[1] D. Mao, Z. Ouyang, J.C. Wang, A photonic-crystal polarizer integrated with the functions of narrow bandpass and narrow transmission angle filtering, Appl. Phys. B 90 (2008) 127–131.
[2] C.M. Snjezana Tomljenovic-Hanic, M.J. de Sterke, Steel, Eggleton Benjamin, Tanaka Yoshinori, Noda Susumu, High-Q cavities in multilayer photonic crystal slabs, Optics Express 15 (25) (2007) 17248–17253.
[3] F. Abel'Es, Recherches Sur La Propagation Des Ondes Electromagnetiques Sinusodales Dans Les Milieux Stratifies. Application Aux Couches Minces, Ann. Phys. 5 (1950) 596–640 706–782.
[4] R. Hooke, Micrographia, The Royal Society, London, 1665. Reprinted By Palo Alto: Octavo (1998), ISBN 1891788027.
[5] I. Newton, Opticks, 4th ed., William Innys, London, 1730. Reprinted By New York: Dover Publications (1952), ISBN 486602052.
[6] Y. Fink, J.N. Winn, S. Fan, C. Chen, J. Michel, J.D. Joannopoulos, E.L. Thomas, A dielectric omnidirectional reflector, Science 282 (1998) 1679.
[7] Y. Fink, D.J. Ripin, S. Fan, C. Chen, J.D. Joannopoulos, E.L. Thomas, Guiding optical light in air using an all-dielectric structure, J. Lightw. Technol. 17 (1999) 2039.
[8] H. Gevorgan, “Optical diodes and omnidirectional reflectors based on one-dimensional quasi-periodic photonic crystals,” Tech. Phys. Let., vol. 34.
[9] S.K. Awasthi, U. Malaviya, S.P. Ojha, Enhancement of omnidirectional total-reflection wavelength range by using one-dimensional ternary photonic band gap material, J. Opt. Soc. Am. B 23 (2006) 2566–2571.
[10] V.I. Kopp, Z.-Q. Zhang, A.Z. Genack, Prog. Quantum Electron. 27 (2003) 369.
[11] R. Wang, J. Dong, D.Y. Xing, Phys. Status Solid 200 (1997) 529.
[12] A. Banerjee, Novel applications of one-dimensional photonic crystal in optical buffering and optical time division multiplexing, Optik 122 (2011) 355–357.
[13] V.Ya. Zyryanov, V.A. Gunyakov, S.A. Myslivets, V.G. Arkhipkin, V.F. Shabanov, Electrooptical switching in a one-dimensional photonic crystal, Mol. Cryst. Liq. Cryst. 488 (2008) 118–126.
[14] M. Sodagar, M. Miri, A.A. Eftekhar, A. Adibi, Optical bistability in a one-dimensional photonic crystal resonator using a reverse-biased pn-junction, Optics Express 23 (2015) 2676–2685.
[15] A. Banerjee, Enhanced refractometric optical sensing by using one-dimensional ternary photonic crystals, Prog. Electromagn. Res. 89 (2009) 11–22.
[16] J.S. Patel, K. Rastani, Electrically controlled polarization independent liquidcrystal crystals Fresnel lens arrays, Opt. Lett. 16 (1991) 532–534.
[17] Wico C.L. Hopman, Student Member, IEEE, Pierre Pottier, Didit Yudistira, Joris van Lith, Paul V. Lambeck, Richard M. De La Rue, Fellow, IEEE, Alfred Driessen, Senior Member, IEEE, Hugo J.W.M. Hoekstra, and Rene M. de Ridder, Member, IEEE, Quasi-One-Dimensional Photonic Crystal as a Compact Building-Block for Refractometric Optical Sensors, journal of selected topics in quantum electronics, vol. 11, pp. 1–11, 2016.
[18] V. Kumar, K.S. Singh, S.P. Ojha, Abnormal behaviour of one-dimensional photonic crystal with defect, Optik 122 (13) (2011) 1183–1187.
[19] W.D. Zhou, J. Sabarinathan, P. Bhattarcharya, et al., Characteristics of a photonic bandgap single defect microcavity electroluminescent device, IEEE J. Quantum Electron. 37 (9) (2001) 1153–1160.
[20] W.D. Zhou, J. Sabarinathan, P. Bhattarcharya, et al., Characteristics of a photonic bandgap single defect microcavity electroluminescent device, IEEE J. Quantum Electron. 37 (9) (2001) 1153–1160.
[21] Z.M. Jiang, B. Shi, D.T. Zhao, J. Liu, X. Wang, Silicon based photonic crystal heterostructure, Appl. Phys. Lett. 79 (21) (2001) 3395–3397.
[22] S. Tomljenovic-Hanic, A. Rahmani, M.J. Steel, C.M. de Sterke, Photonic crystal cavities for sensing: dielectric modes versus air modes, Conference on Lasers and Electro-Optics, 2009 and 2009 Conference on Quantum Electronics and Laser Science Conference. CLEO/QELS 2009. 2009 (2009) 1–2.
[23] Y. Zhao, Y.-N. Zhang, R.-Q. Lv, Simultaneous measurement of magnetic field and temperature based on magnetic fluid infiltrated photonic crystal cavity, IEEE Trans. Instrum. Meas. 64 (2015) 1055–1062.
[24] L. Huang, J. Zhou, F. Sun, Z. Fu, H. Tian, Optimization of one dimensional photonic crystal elliptical-hole low-index mode nanobeam cavities for on-chip sensing, J. Lightw. Technol. IEEE 34 (2016) 3496–3502.
[25] F. Segovia-Chaves, H. Vinck-Posada, Tunable transmittance spectrum in one-dimensional photonic crystals composed of $HgBa_2Ca_2Cu_3O_{8+\delta}/GaAs$ with a defective GaAs layer, Optik 181 (2019) 493–498.
[26] F. Segovia-Chaves, H. Vinck-Posada, Transmittance spectrum in a regular one-dimensional photonic crystal and with the insertion of a $YBa_2Cu_3O_{7x}$ defective layer, Optik 181 (2019) 416–422.
[27] F. Frascella, S. Ricciardi, P. Rivolo, V. Moi, F. Giorgis, E. Descrovi, F. Michelotti, P. Munzert, N. Danz, L. Napione, M. Alvaro, F. Bussolino, A fluorescent one-dimensional photonic crystal for label-free biosensing based on Bloch surface waves, Sensors 13 (2013) 2011–2022.
[28] T. Chen, Z. Han, J. Liu, Z. Hong, Terahertz gas sensing based on a simple one-dimensional photonic crystal cavity with high quality factors, Appl. Opt. 53 (2014) 3454–3458.
[29] J.E. Baker, R. Sriram, B.L. Miller, Two-dimensional photonic crystals for sensitive microscale chemical and biochemical sensing, Lab Chip 21 (2015) 971–990.
[30] F. Segovia-Chaves, H. Vinck-Posada, Dependence of the defect mode with temperature, pressure and angle of incidence in a 1D semiconductor-superconductor photonic crystal, Phys. C: Supercond. Appl. 553 (2018) 1–7.
[31] F. Segovia-Chaves, H. Vinck-Posada, Tuning of the defect mode in a 1D superconductor-semiconductor crystal with hydrostatic pressure dependent frequency of the transverse optical phonons, Phys. C: Supercond. Appl. 556 (2019) 7–13.
[32] P.S. Nunes, N.A. Mortensen, J.P. Kutter, K.B. Mogensen, Refractive index sensor based on a 1-D photonic crystal in a microfluidic channel, Sensors 10 (2010) 2348–2358.
[33] S.E.S. Abd El-Ghany, Temperature sensors based on one dimensional photonic crystals with different double defects, J. Nanoelectron. Optoelectron. 12 (2017) 1–8.
[34] M.H. Lee, H. Gao, T.W. Odom, Refractive index sensing using quasi one-dimensional nanoslit arrays, Nano Lett. 9 (2009) 2584–2588.
[35] A. Motogaito, S. Mito, H. Miyake, K. Hiramatsu, Detecting high-refractive-index media using surface plasmon sensor with one-dimensional metal diffraction grating, Optics Photonics J. 6 (2016) 164–170.
[36] H. Alatas, H. Mayditia, H. Hardhienata, A.A. Iskandar, M.O. Tjia, Single-frequency refractive index sensor based on a finite one-dimensional photonic crystals with two defects, Jpn. J. Appl. Phys. 45 (2006) 6754–6758.
[37] A. Shakoor, M. Grande, J. Grant, D.R.S. Cumming, One-dimensional silicon nitride grating refractive index sensor suitable for integration with CMOS detectors, IEEE Photonics 9 (2017) 1–12.
[38] N.R. Ramanujam, I.S. Amiri, S.A. Taya, S. Olyaee, R. Udaiyakumar, A. Pasumpon Pandian, K.S. Joseph Wilson, P. Mahalakshmi, P.P. Yupapin, Enhanced sensitivity of cancer cell using one dimensional nano composite material coated photonic crystal, Microsyst. Technol. (2018) 1–8, https://doi.org/10.1007/s00542-018-3947-6.
[39] Q. Liu, S. Li, H. Chen, J. Li, Z. Fan, High-sensitivity plasmonic temperature sensor based on photonic crystal fiber coated with nanoscale gold film, Appl. Phys. Exp. 8 (2015) 046701.
[40] X. Quan, E. Fry, Empirical equation for the index of refraction of seawater, Appl. Optics 34 (1995) 3477.
[41] P. Yeh, Optical Waves in Layered Media, Wiley-Interscience, 2005.
[42] S. Orfanidis, Electromagnetic Waves and Antennas, NJ Rutgers University, New Brunswick, 2002.